Biochimica et Biophysica Acta 1807 (2011) 707–718

Contents lists available at ScienceDirect

Biochimica et Biophysica Acta

journal homepage: www.elsevier.com/locate/bbabio

AICAR inhibits cancer cell growth and triggers cell-type distinct effects on OXPHOS biogenesis, oxidative stress and Akt activation ☆

Caroline Jose, Etienne Hébert-Chatelain, Nadège Bellance, Anaïs Larendra, Melser Su, Karine Nouette-Gaulain, Rodrigue Rossignol *

(MRGM) Maladies Rares: Génétique et Métabolisme, F-33076 Bordeaux, France
Université Victor Segalen bordeaux 2, F-33076 Bordeaux, France
Université Bordeaux 1, F-33400 Talence, France

ARTICLE INFO

Article history:
Received 15 August 2010
Received in revised form 19 November 2010
Accepted 2 December 2010
Available online 22 December 2010

Keywords:
Tumor
Mitochondrion
Oxidative phosphorylation
AICAR

ABSTRACT

The AMP-activated protein kinase agonist AICAR mimics a low intracellular energy state and inhibits the proliferation of cancer cells by different mechanisms, which may depend on the bioenergetic signature of these cells. AICAR can also stimulate mitochondrial biogenesis in myoblasts, neurons and HeLa cells. Yet, whether the reactivation of oxidative phosphorylation biogenesis by AICAR contributes to the growth arrest of cancer cells remains undetermined. To investigate this possibility, we looked at the impact of 24- and 48-hour treatments with 750 μM AICAR on human cancer cell lines (HeLa, DU145, and HEPG2), non-cancer cells (EM64, FM14, and HLF), embryonic cells (MRC5) and Rho^0 cells. We determined the bioenergetic profile of these cells and assessed the effect of AICAR on oxidative phosphorylation biogenesis, cell viability and cell proliferation, ROS generation, mitochondrial membrane potential and apoptosis induction. We also followed possible changes in metabolic regulators such as Akt and Hif1-α stabilization which might participate to the anti-proliferative effect of AICAR. Our results demonstrated a strong and cancer-specific anti-growth effect of AICAR that may be explained by three different modes according to cell type: the first mode included stimulation of the mitochondrial apoptotic pathway however with compensatory activation of Akt and upregulation of oxidative phosphorylation. In the second mode of action of AICAR Akt phosphorylation was reduced. In the third mode of action, apoptosis was activated by different pathways. The sensitivity to AICAR was higher in cells with a low steady-state ATP content and a high proliferation rate. This article is part of a Special Issue entitled: Bioenergetics of Cancer.

1. Introduction

The bioenergetic profile of a given tumor can vary widely from glycolytic to oxidative, according to the oncogenes activated and the microenvironment [1–5]. The typical "glycolytic" type of cancer cells presents an enhanced glycolytic machinery confronted to a less efficient OXPHOS system, while the "OXPHOS" type of cancer cells relies mainly on mitochondrial respiration to produce ATP from glucose and glutamine oxidation [6–8]. It was demonstrated that mitochondrial oxidative phosphorylation is of low efficiency in glycolytic tumors, notably through a reduction of mitochondrial content [9–13]. Therapeutic strategies able to interfere specifically with the pathways primarily used by cancer cells for energy production could ideally permit to reduce tumor growth [14,15]. As each cancer cell type presents their own bioenergetic signature [5,16–18], pharmacological attempts to interfere with distinctive steps of cancer energy production pathways could provide drug specificity. Hence, a potential therapeutic strategy may begin with the determination of the bioenergetic signature of tumors [7,10,19–22] followed by the reactivation of the mitochondrial oxidative metabolism in glycolytic tumors with ineffective mitochondria, when appropriate. Indeed, stimulation of PDH activity with sodium-dichloroacetate [23] or overexpression of frataxin [24] reduced the proliferation of colorectal cancer cell lines and colon cancer cells, respectively. Another possibility could consist in the global stimulation of mitochondrial biogenesis in cancer cells with a reduced mitochondrial content and OXPHOS capacity. In a previous study performed on lung epidermoid carcinoma cells we attempted to reactivate mitochondrial biogenesis by using resveratrol [10], a polyphenol that activates Sirt1 and promotes PGC1-α deacetylation,

Abbreviations: ADP, adenosine diphosphate; AICAR, 5-amino-4-imidazolecarboxamide ribonucleoside; ANT, adenine nucleoide translocator; ATP, adenosine triphosphate; COX, cytochrome c oxidase; Cyt c, cytochrome c; CoQ, coenzyme Q; OXPHOS, oxidative phosphorylation; RCR, respiratory control ratio; TMPD, *N,N,N′,N′*-tetramethyl-*p*-phenylenediamine

☆ This article is part of a Special Issue entitled: Bioenergetics of Cancer.

* Corresponding author. (MRGM) Maladies Rares: Génétique et Métabolisme, Université Victor Segalen Bordeaux 2, 146 Rue Léo Saignat 33076 Bordeaux, France.
E-mail address: rossig@u-bordeaux2.fr (R. Rossignol).

0005-2728/$ – see front matter © 2010 Elsevier B.V. All rights reserved.
doi:10.1016/j.bbabio.2010.12.002

resulting in mitochondrial protein expression [25,26]. With resveratrol, we observed a rapid and specific loss of cancer cell viability, while non-cancer lung fibroblasts treated with the same doses presented a stimulation of mitochondrial energy metabolism and increased cell viability [25]. In the present article, we followed on this strategy by using the AMP-activated protein kinase agonist AICAR, which was shown to stimulate mitochondrial biogenesis in skeletal muscle [26,27] and cultured cells as diverse as neurons [28], myocytes [29] and myotubes [26]. In addition, a potent anti-tumoral effect was demonstrated for AICAR in pancreatic cancer cells [30], melanomas [31], cervical cancer [32–34], breast cancer cells [35,36], leukemia-derived lymphoblasts [37], glioblastomas [38], prostate cancer cells [36,39,40], hepatomas [41], myelomas [42], colon and gastric cancer cells [43–45], hematological cell lines [36], C6 gliomas [36], astrocytomas [36,46] and chronic myelogenous leukemia cells [36]. Furthermore, when administered *in vivo*, AICAR attenuated the growth of MDA-MB-231 tumors and of glioblastoma xenografts in nude mice [38,47]. However, eventual changes in mitochondrial or OXPHOS content by AICAR were not investigated as one participating mechanism to the observed anti-proliferative effects of this drug on cancer. In addition to possible changes in OXPHOS biogenesis, AICAR could also modulate cancer cell proliferation by acting on Akt phosphorylation and HIF1α content, both of which are potent regulators of cancer cell proliferation and energetics. Lastly, the reduction of cancer cell viability induced by AICAR might also include the activation of apoptosis, and this mechanism remains to be evaluated.

Here, we analysed the impact of 24- and 48-hour treatments with 750 μM AICAR on the viability of cancer and non-cancer cells. We used tumor-derived cell lines with native differences in their bioenergetic profile as well as Rho^0 cells to evaluate the link between the cellular energy state and the sensitivity to AICAR. To investigate the cell-type specific impact of AICAR in the cell lines tested, we determined changes in OXPHOS content, induction of apoptosis, generation of ROS and activation of the Akt–GS3K survival pathway.

2. Materials and methods

2.1. Chemicals

All the reagents including AICAR (Aminoimidazole-4-carboxamide-1-β-D-ribofuranosyl 5′-monophosphate) were purchased from Sigma-Aldrich, with the exception of the ATP monitoring kit (ATP Bioluminescence Assay Kit HS II from Roche).

2.2. Cell types and culture conditions

HeLa, DU145, HEPG2, HLF and MRC-5 cells were purchased from the American Type Culture Collection (ATCC). The primary monolayer epithelial cell line EM64 and the primary monolayer fibroblasts FM14 were prepared in our laboratory. The primary fibroblasts derived Rho^0 cells were prepared by using 2′3′-dideoxycytidine as we detailed in [48]. A description of each cell line is given in Table 1. Cells were grown in Glucose Dulbecco's Modified Eagle Media (DMEM) containing 25 mM glucose supplemented with 10% fetal bovine serum (*PAA*), 100 U/ml penicillin, and 100 U/ml of streptomycin. All cells were kept in 5% CO_2 at 37 °C. For all experiments cells were harvested during exponential phase of growth at 70% confluency.

2.3. Cell enumeration and cell viability

The cytotoxicity of AICAR was evaluated on the different cell lines by counting the cells after 48 h of treatment with 750 μM AICAR using a Malassez haemocytometer. Cells were seeded in 6 well plates (100 000 cells per well) and treated with 750 μM AICAR for 48 h. Then, cells were trypsinized and counted manually ($N>3$ for each condition). Cell viability was measured using the neutral red assay as detailed by Borenfreund [49,50]. Absorbance was measured in a multi-well scanning spectrophotometer (MP96 from SAFAS) at a wavelength of 540 nm with a reference set at 630 nm. For each condition, multiple replicates ($n>6$) were performed. The results were expressed as percent value of the control absorbance ratio.

2.4. ATP measurements

The intracellular ATP content was measured by using the bioluminescent ATP kit HS II (Roche Applied). Cells treated or not with AICAR were washed with PBS, detached with trypsin and resuspended in DMEM (100 μl of a cell suspension of 2×10^6 cells/ml). For each cell type one aliquot was used to measure the total ATP content, while the second aliquot was treated with antimycin A for 20 min to block mitochondrial ATP synthesis and allow ATP turnover by the ATP consuming processes. In a third aliquot, glycolysis was blocked with 200 μM iodoacetate to evaluate the participation of glycolysis to cellular ATP synthesis. Then, cells were lysed to release the intracellular ATP by using the lysis buffer provided with the kit (equal volume) for 20 min. 100 μl of this lysate was analysed in a 96 well plate luminometer (Luminoskan) using the luciferine–luciferase reaction system provided with the kit. 100 μl of luciferine/ase was injected in the wells and after 10 s of incubation, bioluminescence was read (1 s integration time). Standardization was performed with known quantities of standard ATP provided with the kit measured in the same conditions. The contribution of glycolysis and oxidative phosphorylation to cellular ATP synthesis was obtained by calculating the ratio of the ATP content in cells treated with antimycin (glycolytic ATP remains) to that determined in untreated cells (glycloysis + OXPHOS). The amount of ATP produced by OXPHOS was verified in cells treated with iodoacetate (glycolysis is blocked) and similar results were obtained.

Table 1
Cell lines description and bioenergetic profile.

Cell line	Organ	Cancer-type	Morphology	Age	Gender	Ethnicity	Tumorigenic	Total ATP (pmoles per 1.10^E5 cells)	% Glycolytic ATP
Cancer cell lines									
HeLa	Cervix	Adenocarcinoma	Epithelial	31	Female	Black	n.d.	0.53	79
DU145	Prostate	Carcinoma	Epithelial	69	Male	Caucasian	Yes	0.63	96
HEPG2	Liver	Hepatocellular carcinoma	Epithelial	15	Male	Caucasian	Yes	0.61	76
Non cancer cell lines									
EM64	n.d.	Normal	Epithelial	Adult	n.d.	n.d.	No	0.96	71
FM14	Skin	Normal	Fibroblast	Adult	Female	Caucasian	No	1.40	48
HLF	Lung	Normal from tissue surrounding epidermoid carcinoma	Fibroblast-like	54	Female	Black	No	1.52	54
Rho 0	Skin	BET treated	Epithelial	Adult	Female	Caucasian	No	0.71	100
MRC-5	Lung	Embryonic	Fibroblast	Fetal (14-week old)	Male	Caucasian	No	0.63	95

(n.d.: not determined).

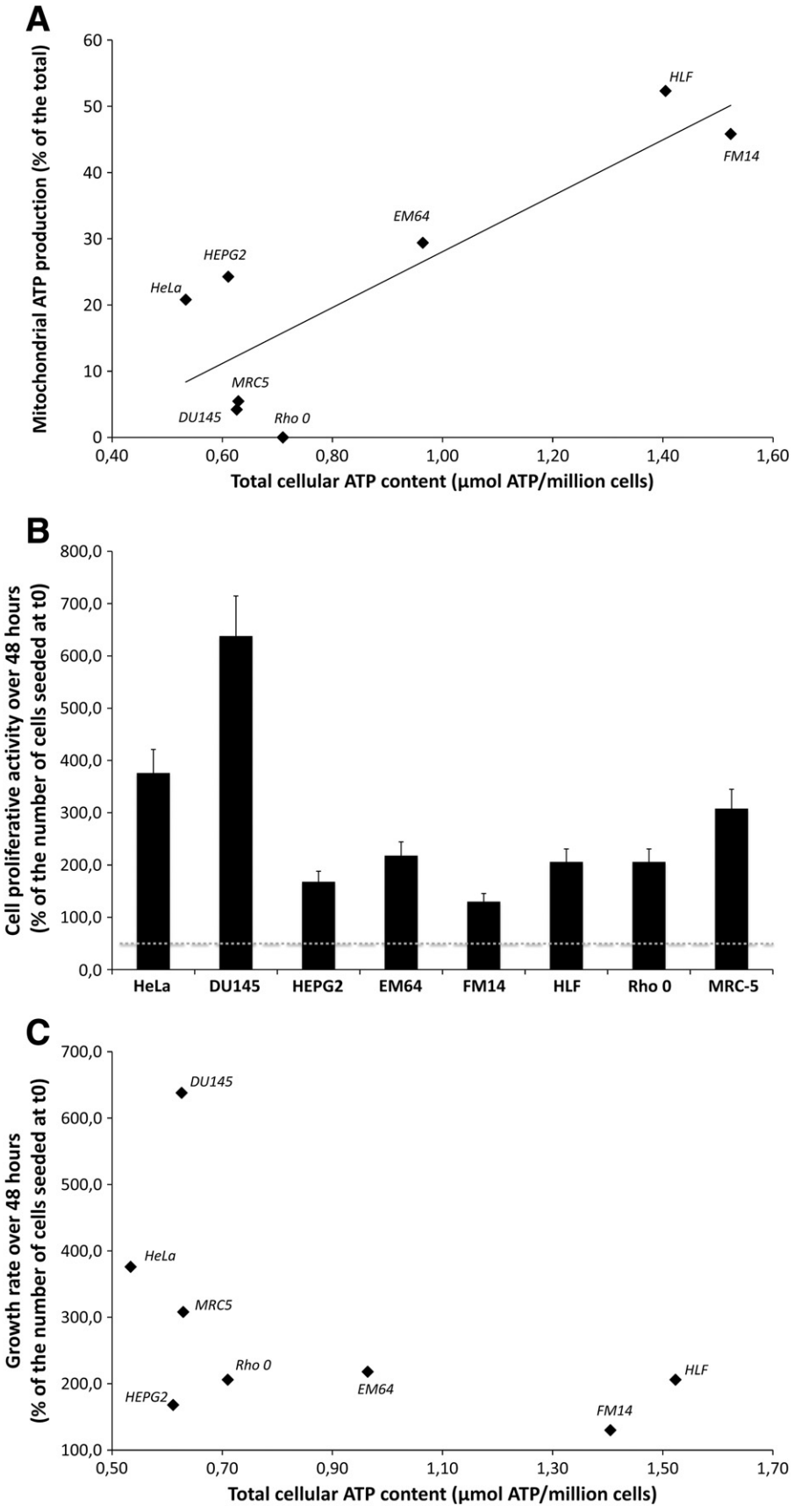

Fig. 1. Growth properties and energy metabolism of cancer cells and non-cancer cells. (A) Correlation between the percentage of mitochondrial ATP production and the total cellular ATP content in the different cell lines. (B) Cell proliferation rate of the different cell lines measured over 48 h; cell culture was initiated with 10 000 cells. (C) Cell growth rate was plotted as a function of the cellular steady-state ATP content. All the data shown correspond to the mean value ± SD of N ≥ 3 different experiments.

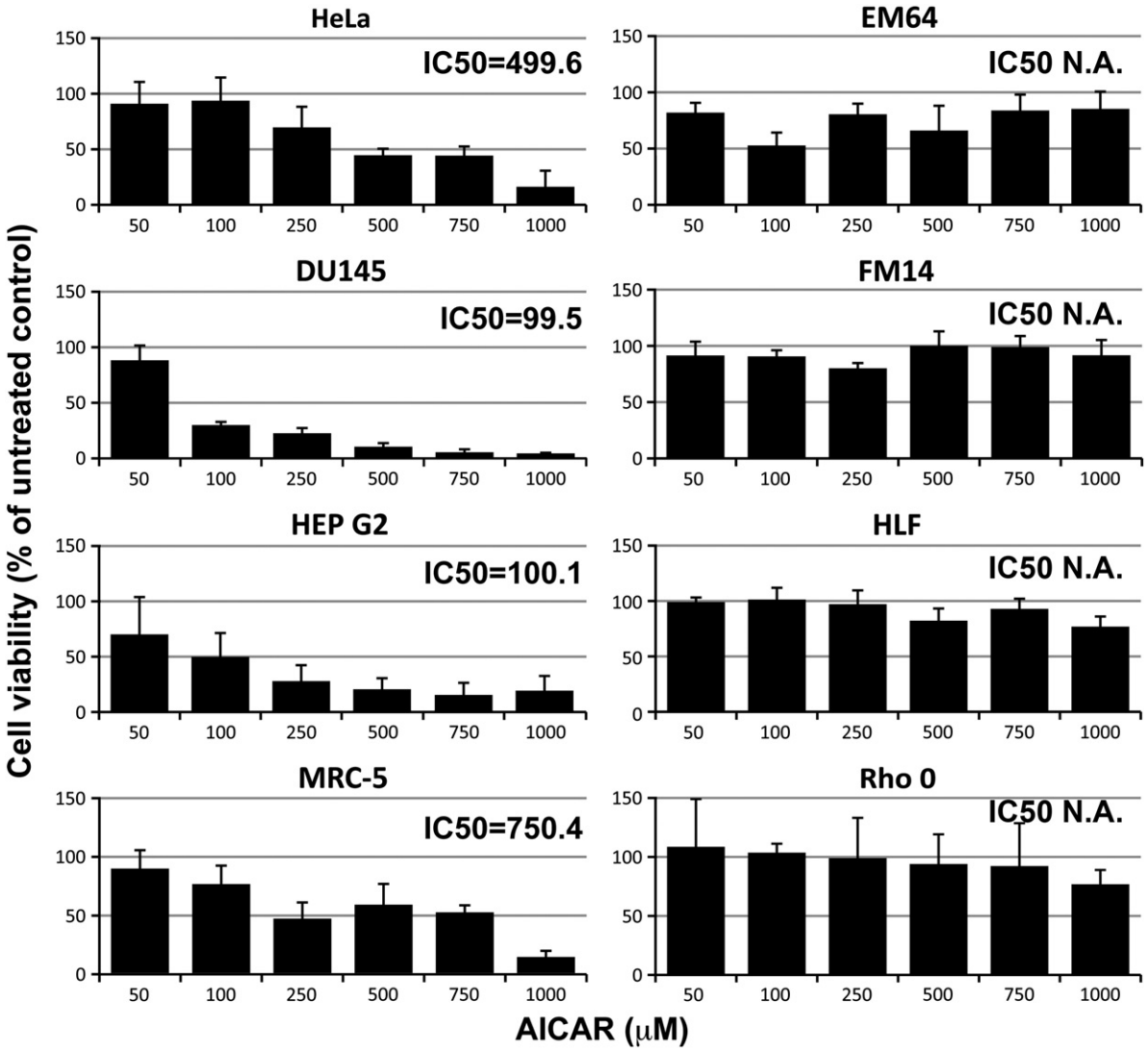

Fig. 2. Impact of a 48 h treatment with 750 μM AICAR on cell viability. The neutral red assay was performed on the different types of cells and the IC_{50} was determined by a fitting procedure (Excel) using a four parameter model. All the data shown correspond to the mean value ± SD of N ≥ 3 different experiments. N.A. = Not Applicable (the data cannot be fitted as no inhibition is observed) in the non-cancer cells.

2.5. Measurement of mitochondrial transmembrane electric potential and ROS cytosolic concentration on cell populations

Cells were trypsinized, counted, and incubated in the presence of 750 μM AICAR for 24 h in DMEM. TMRM (*Invitrogen*) was used for measuring the relative mitochondrial membrane potential. Changes in cytosolic ROS levels were monitored using the CM-H_2DCFDA probe. These probes were added in the cell suspension in the presence of AICAR, and incubated for 30 min at 37 °C, according to the manufacturer's protocol. Cells were washed in PBS, and fluorescence was measured in a quartz cuvette on a Xenius spectrofluorometer (*SAFAS*). A second reading was performed with the addition of 100 μM H_2O_2 in the cuvette to verify the response and the absence of saturation of CM-H_2DCFDA probe. The signal increased immediately after the addition in a dose dependent manner. In the same manner, a second reading was performed with the addition of 100 μM FCCP for the TMRM probe (results not shown) and the signal decreased immediately. The fluorescence value measured after FCCP was close to zero and similar in all the samples tested. We expressed the $\Delta\Psi$ as the difference between TMRM fluorescence measured in the sample and that measured after FCCP addition.

2.6. Assessment of mitochondrial network morphology, and single cell evaluation of ROS level and $\Delta\Psi$ by fluorescence microscopy

Cells were grown in 6 well plates for 24 h in the presence or not of 750 μM AICAR. The mitochondrial network was stained with the Mitotracker green dye (Invitrogen), used at 60 nM for 15 min at 37 °C. Cytosolic ROS were detected with CM-H_2DCFDA (Invitrogen) used at 5 μM for 30 min as detailed in [51] and relative $\Delta\Psi$ was evaluated with TMRM used at 60 nM for 30 min, as described in [51]. The probes were added directly to the wells under the continuous presence of AICAR. For these observations we used a Nikon E 200 microscope, with a 60×, 1.4 N.A water immersion objective. A series of images was acquired using a Q-Imaging Retiga Exi fast 1394 digital camera, driven by Fluo'up (Explora Nova, France). Image analysis was performed with Morpho pro v2.8 (Explora Nova, France).

2.7. Western-blotting

Total cell lysis was performed using 0.4% lauryl-maltoside, for 30 min on ice. Samples were diluted into a SDS-PAGE tricine sample buffer (*Bio-Rad*) containing 2% β-mercaptoethanol by incubation for 30 min at 37 °C, and separated on a 4–20% SDS polyacrylamide

gradient mini-gel (*Bio-Rad*) at 150 V. Proteins (20 μg for each sample) were transferred electrophoretically to 0.45 μm polyvinylidine difluoride (PVDF) membranes for 2 h at 100 mA in CAPS buffer (3.3 g CAPS, 1.5 l 10% methanol, pH 11) on ice. Membranes were blocked overnight in 5% milk-PBS + 0.02% azide, and incubated for 4 h with the primary antibodies. Polyclonal antibodies against caspase 3, PARP, phospho-Akt-Ser473 and phospho-GS3Kβ and monoclonal antibodies against Hif1α, β-actin, MnSOD were obtained from Santa Cruz Biotechnology. Monoclonal antibodies against respiratory chain complexes were obtained from Mitosciences (OXPHOS cocktail). After six washes with PBS − 0.05% Tween 20, the membranes were incubated for 1 h with horseradish peroxidase-conjugated goat anti-rabbit (*Bio-Rad*), or bovine anti-goat diluted in 5% milk-PBS. This secondary antibody was detected in a Chemidoc (biorad) using the chemiluminescent ECL PlusTM reagent (*Amersham*). The signal was quantified by densitometric analysis using Image J (*NIH*) software.

2.8. Statistical analysis

All the data presented in this study correspond to the mean value of N experiments ± SD, with N ≥ 3. Comparison of the data sets (control versus AICAR treated) was performed with the Student's t test, using Excel Software (*Microsoft*). Two sets of data were considered statistically different when $P<0.05$.

3. Results

3.1. Metabolic profile of the tumor-derived cell lines and of the primary cells

We measured the relative contribution of glycolysis and of oxidative phosphorylation (OXPHOS) to the cellular ATP production (Table 1). This was obtained by using specific inhibitors of glycolysis (iodoacetate) and of OXPHOS (antimycin). In Table 1, the tissue of origin and the type of tumor from which the cancer cell lines originated are specified. It can be seen that all the tumor-derived cell lines used in this study produced their vital ATP mainly through glycolysis (from 76 to 96% of the total ATP produced), while non-cancer cells relied on glycolysis to a lesser extent (from 48 to 71%). As expected, the Rho^0 cells, depleted of mitochondrial DNA, relied exclusively on glycolysis to produce ATP. The embryonic lung fibroblasts (MRC-5) also used glycolysis to a large extent (95%). The total ATP content was higher in non-cancer cells (HLF, EM64 and FM14) as compared to cancer cells, which positively correlated ($R^2 = 0.71$, $p = 0.0148$) with the degree of OXPHOS utilization for ATP synthesis (Fig. 1A). The rate of cell proliferation was evaluated by measuring the net increase in cell number after 48 h of growth (Fig. 1B). HeLa and DU145 were fast-growing cancer cell lines in contrast with HEPG2. The non-cancer cells (FM14, EM64 and HLF) showed a lower rate of cell proliferation (mean value of 50% increase in cell number after 48 h) as compared to the cancer group (294%). The embryonic cell line MRC-5 presented a rather high proliferation rate (208%) intermediate between the cancer cells and the control cells, as was the case of Rho^0 (106%). Lastly, cells with a high proliferation rate showed low steady-state values of total ATP content, and reciprocally (Fig. 1C).

3.2. AICAR treatment decreases proliferation and viability of cancer cells

We treated the different cell-lines with increasing concentrations of AICAR (from 50 μM to 1 mM) for 48 h and measured cell viability using the neutral red assay (Fig. 2A–H). AICAR was present during all the measurements described below (continuous AICAR treatment).

The calculated IC_{50} values for AICAR are given in Fig. 2. In striking contrast with the non-cancer cells and the Rho^0 cells, we observed a clear dose-dependent inhibition of neutral red uptake in all the cancer cells tested (IC_{50} values ranging from 99 to 500 μM) and in the embryonic cell line ($IC_{50} = 750$ μM), suggesting a decrease in viability upon treatment of cancer cells with AICAR. As the neutral red uptake test depends both on cell number and cell metabolic activity, we assessed the actual decrease in cell number induced by AICAR (Fig. 3). We observed no increase in the number of dead cells in the culture dishes at 12, 24 and 48 h (data not shown). Instead, AICAR treatment strongly reduced the proliferation of cancer cells (HeLa, DU145 and HEPG2) after 48 h of treatment (55, 95 and 85% of inhibition respectively), while no significant or little effect was observed for the non-cancer epithelial cells EM64, skin fibroblasts FM14 and HLF (16, 1 and 7% of inhibition respectively). The embryonic non-cancer cell line MRC-5 showed a strong decrease in cell number (55% of inhibition). A comparison of the effect of AICAR on cell number and cell viability (Fig. 3) indicated a stronger effect of AICAR on the latter. For instance, the prostate cancer cell line DU145 showed a reduction by 70 ± 06% of the cell number, while viability was reduced by 95 ± 03%.

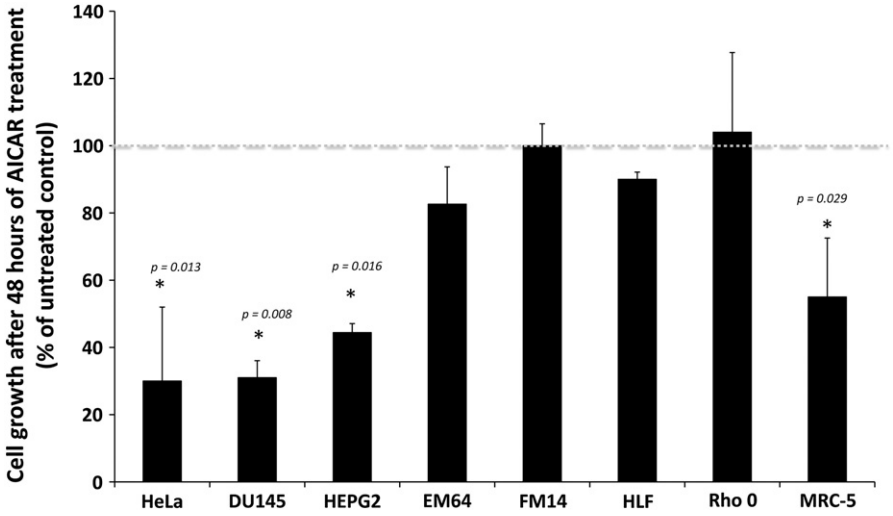

Fig. 3. Effect of AICAR on cell number (after 48 hours of growth.). The results are expressed as percentage of cell viability or cell number obtained in the untreated controls. All the data shown correspond to the mean value ± SD of N ≥ 3 different experiments. *p* values were obtained from the comparison of the AICAR treated samples with the untreated ones.

3.3. Impact of AICAR treatment on apoptosis and cell survival

We evaluated the degree of apoptosis induction by measuring the increase in caspase 3 and PARP protein content (active forms) after treatment of the cell lines with 750 μM AICAR for 24 h (Fig. 4A and B). Although the inactive (uncleaved) form of PARP was observed in all the cell lines at the exception of FM14 and HEPG2, its active form was only detected in HLF cells under normal conditions. In HLF, AICAR treatment induced an increase (363%, $p<0.05$) in the active form of PARP, as well as that of caspase 3 (825% of the untreated control, $p<0.05$). Interestingly, Akt phosphorylation at serine 473 was increased in HeLa, MRC-5 and HLF (140, 126 and 163% of the untreated control, respectively). In contrast, Akt phosphorylation (activation) was significantly reduced in DU145 and HEPG2. We also looked at the overall morphology of the mitochondrial network (Fig. 5) which typically harbors a fragmented shape when apoptosis is induced [52]. In accordance with the levels of PARP and caspase-3, no sign of fragmentation of the mitochondrial network was noticed at 4 h, 8 h, 12 h 24 h and 48 h in the cell-lines following the treatment with AICAR (in this figure the 24 h data are shown). The Rho^0 cells show a fragmented mitochondrial network in the control conditions, and no further fragmentation was observed after the AICAR treatment.

3.4. Impact of AICAR treatment on the cell cycle regulator GSK3β

Glycogen synthase kinase-3beta (GSK3β) generally represses cell cycle progression by direct phosphorylation of cyclin D1 [53]. As AICAR treatment inhibited the proliferation in cancer cells, we measured possible changes in the phosphorylation status of GSK3β by western-blot (Fig. 4A and C). We observed a significant increase in GSK3β phosphorylation in EM64, DU145 and HeLa cells (286, 167 and 131% of the untreated control, respectively). In contrast, GS3Kβ phosphorylation was reduced in Rho^0, HEPG2 and HLF cells (64, 32 and 53% of the untreated control, respectively).

3.5. Modulation of OXPHOS content by AICAR

The expression level of five mitochondrial respiratory chain proteins was evaluated by western blot and the individual modifications (mean ± SD values and p values) are given in (Fig. 6A and B). In MRC-5 and HeLa cells treated with 750 μM AICAR there was a significant increase ($p<0.05$) in the levels of (+22% mean value). Conversely, in EM64, DU145 and Rho^0 cells, there was a significant reduction (−22% mean value, $P<0.05$). We also tested the impact of the AICAR treatment on Hif1α as this transcription factor plays a central role in the metabolic remodeling of cancer cells. Hif1α was

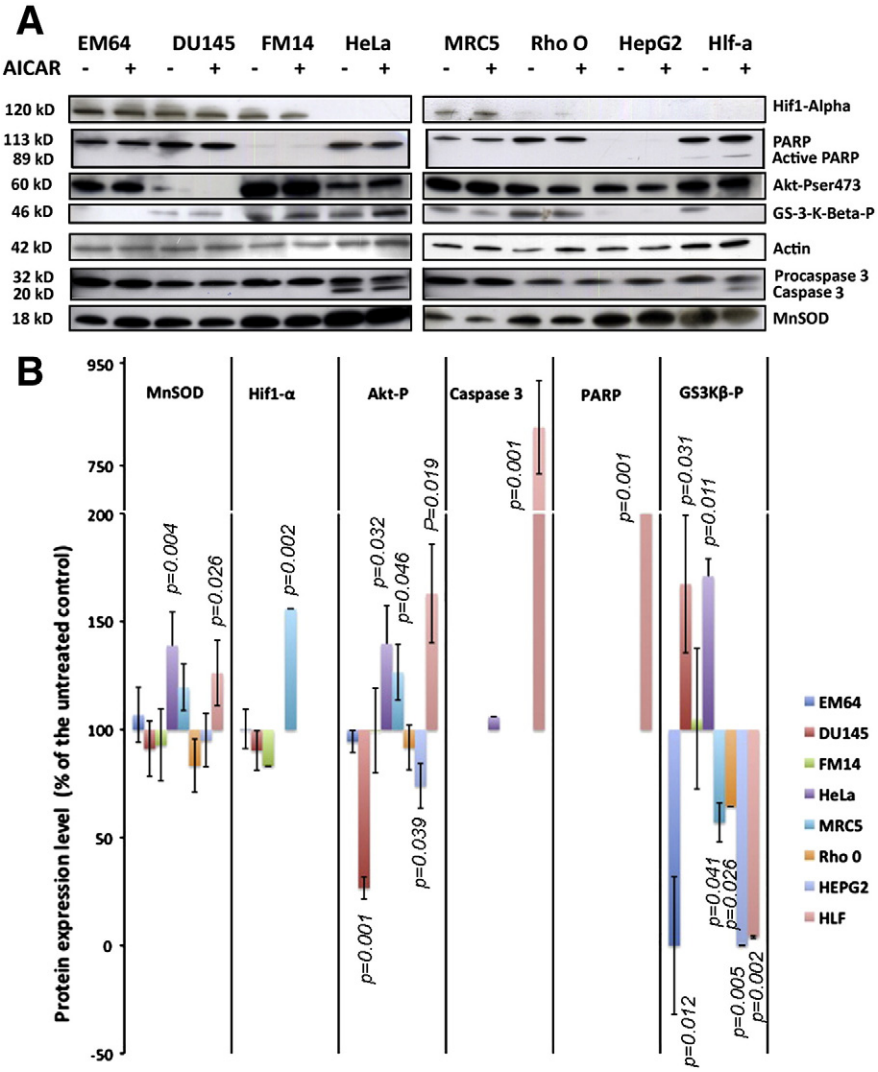

Fig. 4. Effect of AICAR on apoptosis and cell survival. (A) Western blot analyses performed on 20 μg of proteins taken from cell treated with 750 μM AICAR for 48 h. (B) Protein expression levels (normalized to actin) of signaling and apoptosis proteins in cell treated with 750 μM AICAR for 24 h. All the data shown correspond to the mean value ± SD of N ≥ 3 different experiments. p values were obtained from the comparison of the AICAR treated samples with the untreated ones.

only detectable in four cell lines (Fig. 4A) and the AICAR treatment triggered a significant increase ($P<0.05$) of its content (+56%) solely in the embryonic MRC-5 fibroblasts.

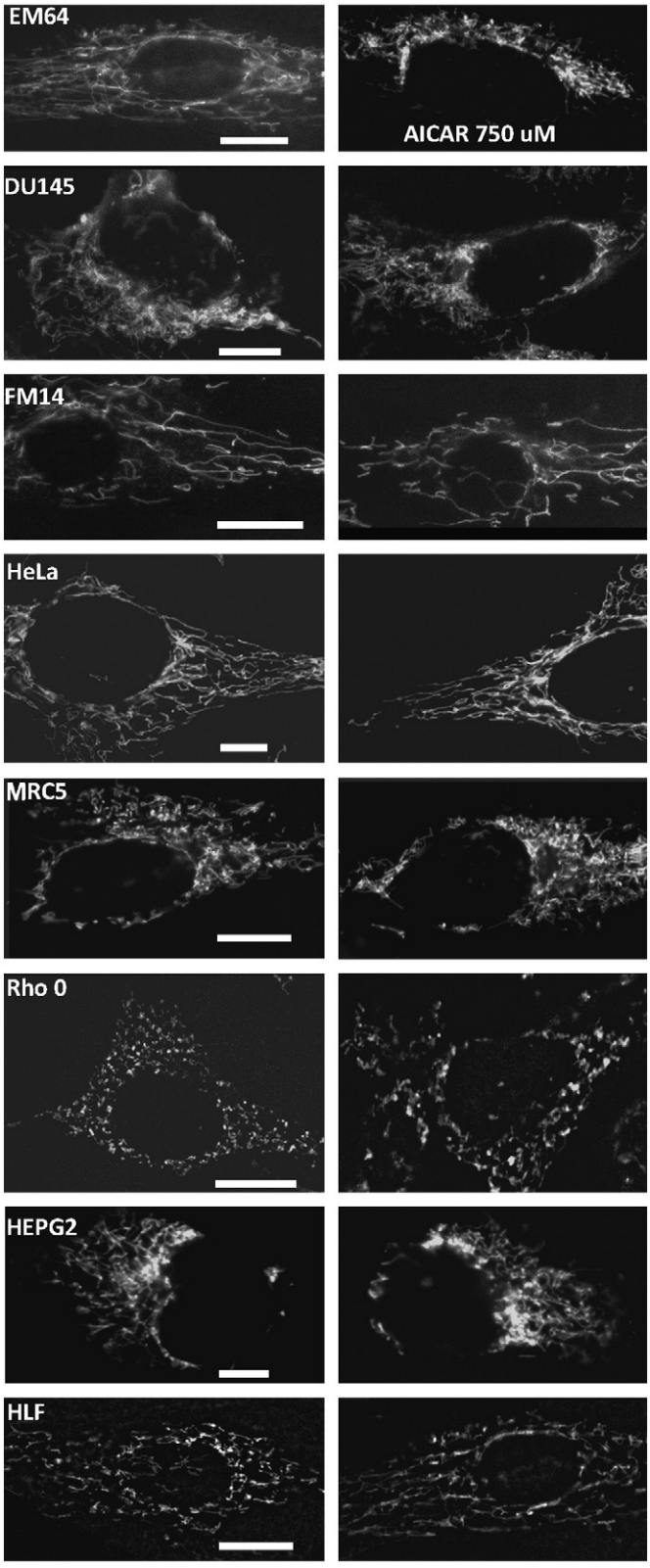

Fig. 5. Impact of AICAR on the fragmentation of the mitochondrial network. The mitochondrial network was stained with Mitotracker Green in cells treated (right panel) or not (left panel) for 24 h with 750 μM AICAR. No sign of mitochondrial fragmentation was observed in all the cells except for the Rho^0 cells where the untreated controls exhibited a fragmented mitochondrial network.

3.6. Effect of AICAR on oxidative stress and antioxidant defenses

To evaluate changes in oxidative stress possibly mediated by the AICAR treatment we monitored intracellular DCFDA-detectable oxidants production by measuring CM-H_2DCFDA fluorescence (Fig. 7A). A significant reduction ($P<0.05$) of CM-H_2DCFDA fluorescence was noticed in HeLa cells (−50%), FM14 cells (−66%) and MRC-5 cells (−29%). This was correlated with a significant increase in the expression level of MnSOD (Fig. 4A and B) in HeLa cells (+ 39%) and MRC5 cells (+20%). Conversely, in HEPG2, EM64, HLF and Rho^0 cells the AICAR treatment induced a significant increase in ROS levels (ranging from 29% in HEPG2 to 51% in HLF). Fluorescence microscopy analyses (Fig. 7B) revealed the presence of ROS in the cytosol and the mitochondrion, as confirmed with the co-staining of DU 145 cells with CM-H_2DCFDA and TMRM (Fig. 7B lower panel).

3.7. Effect of AICAR on mitochondrial membrane potential ($\Delta\Psi$)

Moderate changes in mitochondrial $\Delta\Psi$ reflect variations in respiratory chain activity, while a large drop in $\Delta\Psi$ can indicate the onset of apoptosis. Here, we monitored the relative changes in $\Delta\Psi$ after 24 h of treatment with 750 μM AICAR by measuring TMRM fluorescence (Fig. 8). The results showed a significant decrease of $\Delta\Psi$ in DU145 (−16%), HEPG2 (8%), EM64 (−25%) and FM14 (−14%). Conversely, TMRM fluorescence was increased in HeLa cells (+27%), HLF cells (+16%) and Rho^0 cells (+12%). We verified that in our experimental conditions TMRM entered the mitochondrion and did not show unspecific staining (data not shown).

4. Discussion

The main findings of our study are the strong inhibition of cancer cell's viability and proliferation by AICAR without affecting non-cancer cell's viability and proliferation. Numerous studies have reported the anti-proliferative effect of AICAR on cancer cells but often lacked a comparison with paired non-cancer cells, and therefore data about cancer-specificity of AICAR must be used with caution. Our data indicate a strong effect of AICAR on the cancer prostate carcinoma cell line DU145 and the hepatocellular carcinoma HEPG2 cell line (IC_{50} of 100 μM). The epidermoid carcinoma HeLa cells were less sensitive to this treatment (IC_{50} of 500 μM) as was the embryonic cell line MRC-5 (IC_{50} of 750 μM). All these cells share in common a high contribution of glycolysis to the cellular ATP production (ranging from 76% in HEPG2 to 96% in DU145) and a low steady-state ATP content, as compared to the non-cancer cells used in our study and that were not affected by AICAR. This suggests that cells with low steady-state ATP content are more sensitive to AICAR. Cells with the highest sensitivity to AICAR were also those in which (i) the contribution of OXPHOS to ATP synthesis was low, and (ii) cell proliferation rate was rapid, suggesting that cancer cells of the glycolytic type could be preferentially targeted by treatment with AICAR-type compounds. Not surprisingly, the growth of the embryonic cell line MRC-5 was also inhibited by AICAR as previous studies have reported similarities between embryonic cells and cancer cells, with regard to the regulation of energy metabolism. Accordingly, it would be expected that a high mitochondrial bioenergetic activity would protect against the anti-proliferative effect of AICAR [54]. In our study, we observed that cancer cells present a higher proliferation rate as compared to the non-cancer cells. Yet, differences in the tissue of origin and the type of oncogene activated as well as disparities in the preferential energy substrate could explain differences in the observed proliferation rates.

No sign of cell death was observed in the cancer group during the AICAR treatment, as well as no induction of apoptosis, as verified by the absence of caspase 3 and PARP activation or the lack of mitochondrial network fragmentation and deep decrease in $\Delta\Psi$ at

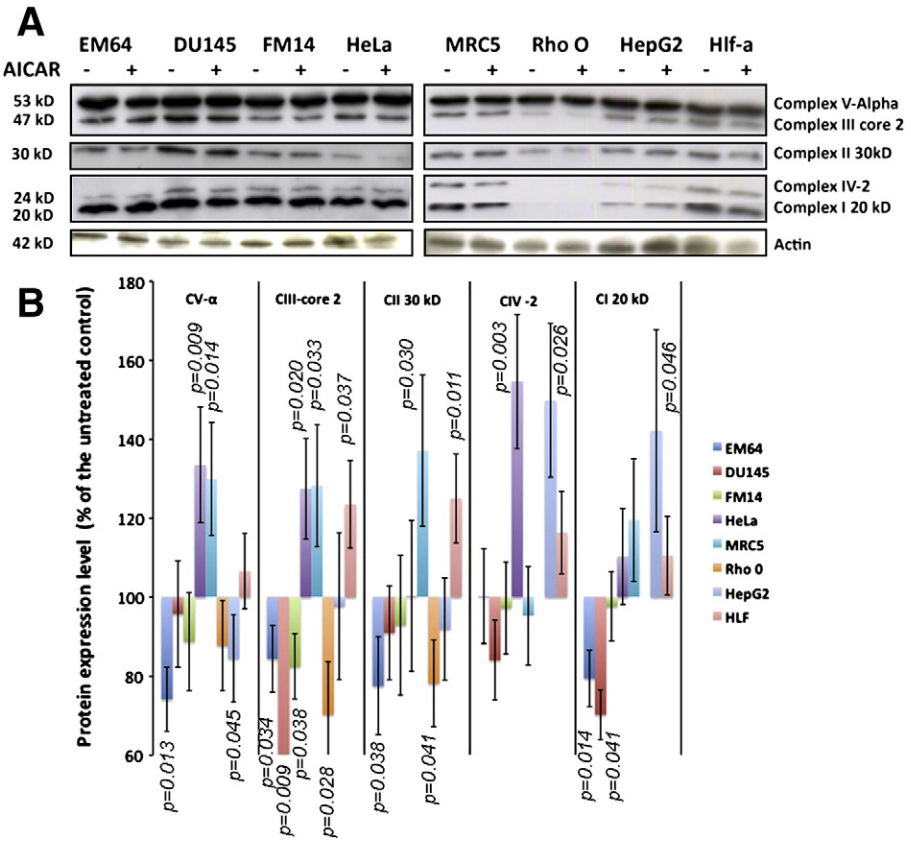

Fig. 6. Effect of AICAR on OXPHOS biogenesis. (A) Western blot analyses performed on 20 μg of proteins taken from cell treated with 750 μM AICAR for 48 h. (B) Densitometric analyses of the expression level of five mitochondrial respiratory chain proteins normalized to the actin levels. All the data shown correspond to the mean value ± SD of N ≥ 3 different experiments. The *p* values (Student t test) are given for each bar. *p* values were obtained from the comparison of the AICAR treated samples with the untreated ones.

the exception of HLF cells. Therefore, the low number of cells observed after the 48 h treatment with 750 μM AICAR can be attributed to a lowered rate of cell proliferation, as previously reported on different cancer cell lines [30,33,37].

The main question we intended to address in our study was the impact of the AICAR treatment on mitochondrial biogenesis in cancer cells and non-cancer cells. To do so we measured the changes in the expression level of five mitochondrial respiratory chain proteins after treatment with AICAR. The effects of AICAR on OXPHOS content were cell-type specific. We found an increase in OXPHOS components in HeLa, MRC-5 (around 30 to 50% increase) and HLF cells (20% increase), while a reduced level of these proteins was observed in EM64, FM14, DU145 and Rho^0 cells (around −20%). Therefore, our observations indicate that the preferential anti-proliferative effect of AICAR on cancer cells did not include a consistent stimulation of OXPHOS biogenesis, in contrast with our hypothesis. Likewise, the observed increase in ROS levels in EM64 and HLF cells was not associated with the sensitivity to AICAR, in comparison with other cell lines tested [55]. However, we did observe an antioxidant effect in HeLa and MRC-5 cells. The activation of Akt by AICAR followed a similar cell-type specific pattern, as Akt phosphorylation was increased in HeLa cells (+50%), MRC5 cells and HLF cells, but it was reduced in DU145 and HEPG2. Sengupta et al. [37] proposed that Akt activation induced by AICAR may represent a compensatory survival mechanism in response to apoptosis and/or cell cycle arrest triggered by this drug. Our observations also suggest that cancer cell elimination might be obtained by using AICAR in combination with Akt inhibitors.

Overall, our study evidenced clear differences in the effect of AICAR on apoptosis induction, mitochondrial biogenesis stimulation, ROS generation and Akt activation, which clearly indicate a cell-type specific response to the AICAR treatment. As deduced from different studies and from our data, three mechanisms could explain the anti-cancer properties of AICAR (Table 2). The first mechanism includes cell cycle arrest and stimulation of the mitochondrial apoptotic pathway with compensatory activation of Akt and stimulation of OXPHOS biogenesis. This mechanism was recently described in leukemia cells [37] and HeLa cells [33]. The second mode of action of AICAR also includes cell proliferation arrest, but Akt phosphorylation is reduced instead of being activated. Consequently, this second mechanism can be observed in cancer cells where Akt was primarily activated, and for which glycolysis is also typically up-regulated [56]. In the third mode of action of AICAR, cancer cells die from apoptosis, as mediated by different pathways (Table 2). Yet, although previous studies indicated the possible activation of apoptosis by AICAR, our results evidenced no significant changes in caspase 3 cleavage upon AICAR treatment. The apparent discrepancy observed between our results and the studies listed in Table 2, with regard to the possible activation of apoptosis by AICAR, might be explained by differences in the type of cancer cells investigated which may present variable dysregulation of the apoptotic pathways.

In our study, the impact of AICAR on DU145 and HEPG2 cells presented similarities with the second mechanism, as cell proliferation was reduced and a reduction of Akt was also observed. HeLa cells followed the first mode of action of AICAR since Akt was activated by AICAR, and induction of apoptosis was not observed. Lastly, HLF cells showed an increased apoptosis with an increased activation of Akt, which resembles the third mechanism. HLF cells are lung non-cancer, as are MRC5, and both demonstrated changes in cell proliferation and Akt after the AICAR treatment, which suggests that AICAR does not target specifically cancer cells. Indeed, the state of Akt activation, cell

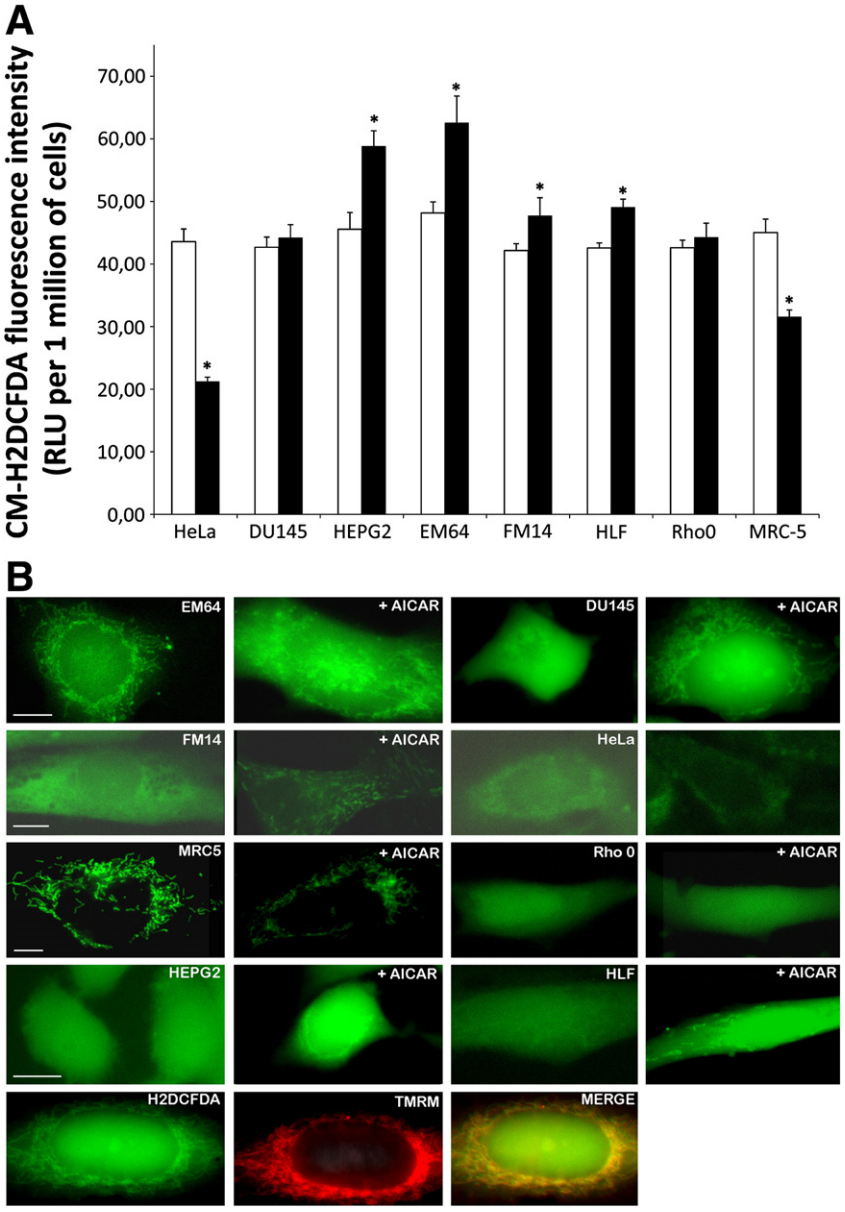

Fig. 7. Effect of AICAR on oxidative stress. (A) Intracellular ROS levels were determined using the fluorescent probe CM-H_2DCFDA on $0.5 \times 1E5$ cells/ml after 24 h of treatment with 750 μM AICAR. * $P \leq 0.05$. (B) CM-H_2DCFDA measurement by fluorescence microscopy in single cells after 24 h of treatment with 750 μM AICAR. All the data shown correspond to the mean value ± SD of $N \geq 3$ different experiments.

proliferation rate and glycolysis utilization might determine more the sensitivity to AICAR, rather than the sole cancer origin of the cell exposed to this drug. This might explain the important undesired effect of this drug in clinical trials [57].

The changes in mitochondrial respiratory chain content following AICAR treatment revealed cell specific responses with large variations. First, we observed an increased content of OXPHOS proteins in cancer (HeLa) and non-cancer cells (MRC5 and HLF) where AICAR also activated Akt and triggered a stimulation of MnSOD expression. A previous study performed on endothelial cells also showed that AICAR stimulates both the expression of MnSOD and increases OXPHOS content through the activation of the AMPK-PGC1α pathway [55]. In HeLa, MRC-5 and HLF all the respiratory chain proteins analysed showed an increased expression, while in HEPG2 the increase was only observed for complex I and complex IV. However, the reduction of respiratory chain content observed in DU145, Rho^0 and EM64 suggests the inhibition of OXPHOS or the activation of mitophagy. Therefore, AICAR can trigger two opposite responses in different cell lines, but their determinants remain unclear. We think that the bioenergetic profile of the cell and its capacity to adapt the energy producing machinery to a low energy-state vary widely between different cell types, explaining the differences of AICAR effects which mimic such a low energy-state. For instance, we observed recently that breast cancer cells reduce their mitochondrial content in hypoxic conditions, while the corresponding non-cancer cells present an opposite increased mitochondrial content [22]. In particular, our study of the impact of AICAR on different cell types evidenced a stronger anti-growth effect on cells with more active proliferation and a low steady-state ATP content, which might reflect an active anabolism and a strong energy need, with a corresponding capacity for bioenergetic adaptation. Interestingly, the Rho^0 cells which solely rely on glycolysis to survive were not affected by the AICAR treatment, indicating that the pathway primarily used for energy production does not determine by itself the sensitivity to AICAR. The

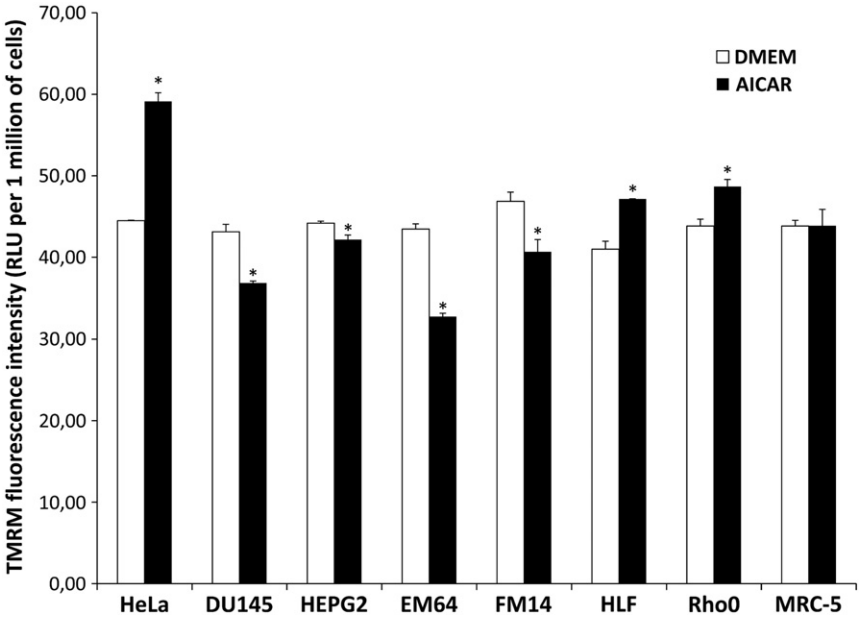

Fig. 8. Effect of AICAR on mitochondrial membrane potential. Mitochondrial membrane potential was determined using the fluorescent probe TMRM on 0.5 × 1E5 cells/ml after 24 h of treatment with 750 μM AICAR. * $P \leq 0.05$. All the data shown correspond to the mean value ± SD of $N \geq 3$ different experiments.

measurements of $\Delta\Psi$ in cells treated with AICAR also showed variable effects according to the type of cells investigated. Instead, as discussed above, the energy status of the cell might determine the impact of AICAR on a given cell line. Likewise, cancer cells and non-cancer cells adapt differently to an increase in energy demand induced by glucose deprivation or oxygen low availability, as occurs in solid tumors [21,22].

5. Conclusions

Our data show that AICAR inhibits the growth of cancer cells in a cell line specific manner. The activation of OXPHOS biogenesis by AICAR is not a consistent property of this drug as the mitochondrial content was even reduced in three cell lines treated with AICAR. The diversity of mechanisms by which AICAR inhibits cancer cell proliferation allows distinguishing three modes of action which may depend on cell line specific energy status and bioenergetic profile. Our study complements that by Mukherjee and colleagues [41] reinforcing the conclusion that cancer cells and non-cancer cells are differentially affected by AICAR, and our results further indicate that AICAR increases OXPHOS content in a subset of cancer cells. In clinical trials, AICAR has proven highly toxic [57] and produces undesired metabolic effects that limit its utilization in cancer therapies. Yet, the strategy of mimicking a low-energy state in cancer cells to trigger cell proliferation arrest and apoptosis is still valid, and the research for identifying novel energy restriction-mimetic agents (ERMAs) [58] capable of reducing human tumor growth will benefit from a better characterization of the bioenergetic signature of cancer cell lines, in particular in response to challenging energy conditions, as occurs during hypoxia and aglycemia.

Table 2
Cell-type dependent modes of action of AICAR.

Apoptosis	Akt activation	Mt-biogenesis	ROS	Cell death	Cell proliferation	Ref.	Cell-type	AICAR mode of action
↑	↑	n.d.	↑↓		↓ p27 p53 (up)	[36]	Leukemia	No. 1
↑		n.d.			↓	[32]	HeLa	
–	↑	↑	↓		↓	present	HeLa	
–	↑	↑	–		↓		MRC5	
	↓	n.d.			↓	[29]	Pancreas	No. 2
↑ p53	↓	n.d.		↑	↓ mTOR (down)	[27]	Cervical	
	↓	n.d.			↓ p21, 27, 53 (up)	[35]	Various	
	↓	n.d.			↓ ERK–S6K–mTOR (down)	[41]	Myeloma	
–	↓	↓	↑		↓	present	DU145	
–	↓	↓	↑		↓		HEPG2	
		n.d.			↓	[46]	Breast	
		n.d.			↓	[38]	Prostate	
		n.d.			p21 (up)–lipogenesis–mTOR (down)	[39]	Prostate	
		Glycolysis ↓			↓ lipogenesis down	[37]	Glioblastoma (EGFR+)	
↑		n.d.		↑		[30]	Melanomas	No. 3
↑ NF-kappaB		n.d.	↑	↑		[58]	Neuroblastoma	
↑ Trail		n.d.		↑		[34]	Breast	
↑		n.d.				[40]	Brain tumor	
↑ p53–p38–cjun		n.d.				[42]	Colon cancer	
↑		n.d.				[43]	Colon cancer	
↑		n.d.				[44]	Gastric cancer	
↑		n.d.				[45]	Astrocytoma	

(n.d.: not determined).

Acknowledgements

We thank the French National Institute for Scientific and Medical Research (INSERM), Université Victor Segalen Bordeaux 2, Région Aquitaine, Ammi, and Cancéropôle Grand Sud-Ouest for financial support. C. Jose was supported by a grant from the FQRNT (Fond Québecois de la Recherche sur la Nature et les Technologies), E. Hébert Chatelain by a grant from the Natural Sciences and Engineering Research Council of Canada, N. Bellance by a grant from INSERM/Région Aquitaine, and G. Benard by a grant from ANR.

References

[1] A. Isidoro, M. Martinez, P.L. Fernandez, A.D. Ortega, G. Santamaria, M. Chamorro, J.C. Reed, J.M. Cuezva, Alteration of the bioenergetic phenotype of mitochondria is a hallmark of breast, gastric, lung and oesophageal cancer, Biochem J 378 (2004) 17–20.
[2] X.L. Zu, M. Guppy, Cancer metabolism: facts, fantasy, and fiction, Biochem Biophys Res Commun 313 (2004) 459–465.
[3] R. Moreno-Sanchez, S. Rodriguez-Enriquez, A. Marin-Hernandez, E. Saavedra, Energy metabolism in tumor cells, FEBS J 274 (2007) 1393–1418.
[4] F. Weinberg, N.S. Chandel, Mitochondrial metabolism and cancer, Ann NY Acad Sci 1177 (2009) 66–73.
[5] K. Smolkova, L. Plecita-Hlavata, N. Bellance, G. Benard, R. Rossignol, P. Jezek, Waves of gene regulation suppress and then restore oxidative phosphorylation in cancer cells, Int J Biochem Cell Biol (2010).
[6] M. Guppy, P. Leedman, X. Zu, V. Russell, Contribution by different fuels and metabolic pathways to the total ATP turnover of proliferating MCF-7 breast cancer cells, Biochem J 364 (2002) 309–315.
[7] S. Rodriguez-Enriquez, L. Carreno-Fuentes, J.C. Gallardo-Perez, E. Saavedra, H. Quezada, A. Vega, A. Marin-Hernandez, V. Olin-Sandoval, M.E. Torres-Marquez, R. Moreno-Sanchez, Oxidative phosphorylation is impaired by prolonged hypoxia in breast and possibly in cervix carcinoma, Int J Biochem Cell Biol (2010).
[8] L. Reitzer, B. Wice, D. Kennel, Evidence that glutamine, not sugar, is the major energy source for cultured Hela cells, JBC 254 (1979) 2669–2676.
[9] E. Hervouet, A. Cizkova, J. Demont, A. Vojtiskova, P. Pecina, N.L. Franssen-van Hal, J. Keijer, H. Simonnet, R. Ivanek, S. Kmoch, C. Godinot, J. Houstek, HIF and reactive oxygen species regulate oxidative phosphorylation in cancer, Carcinogenesis 29 (2008) 1528–1537.
[10] N. Bellance, G. Benard, F. Furt, H. Begueret, K. Smolkova, E. Passerieux, J.P. Delage, J.M. Baste, P. Moreau, R. Rossignol, Bioenergetics of lung tumors: alteration of mitochondrial biogenesis and respiratory capacity, Int J Biochem Cell Biol 41 (2009) 2566–2577.
[11] M. Sanchez-Arago, M. Chamorro, J.M. Cuezva, Selection of cancer cells with repressed mitochondria triggers colon cancer progression, Carcinogenesis 31 (2010) 567–576.
[12] P. Acebo, D. Giner, P. Calvo, A. Blanco-Rivero, A.D. Ortega, P.L. Fernandez, G. Roncador, E. Fernandez-Malave, M. Chamorro, J.M. Cuezva, Cancer abolishes the tissue type-specific differences in the phenotype of energetic metabolism, Transl Oncol 2 (2009) 138–145.
[13] E. Hervouet, J. Demont, P. Pecina, A. Vojtiskova, J. Houstek, H. Simonnet, C. Godinot, A new role for the von Hippel–Lindau tumor suppressor protein: stimulation of mitochondrial oxidative phosphorylation complex biogenesis, Carcinogenesis 26 (2005) 531–539.
[14] L. Galluzzi, N. Larochette, N. Zamzami, G. Kroemer, Mitochondria as therapeutic targets for cancer chemotherapy, Oncogene 25 (2006) 4812–4830.
[15] S. Rodriguez-Enriquez, A. Marin-Hernandez, J.C. Gallardo-Perez, L. Carreno-Fuentes, R. Moreno-Sanchez, Targeting of cancer energy metabolism, Mol Nutr Food Res 53 (2009) 29–48.
[16] P.L. Pedersen, Tumor mitochondria and the bioenergetics of cancer cells, Prog Exp Tumor Res 22 (1978) 190–274.
[17] N. Bellance, P. Lestienne, R. Rossignol, Mitochondria: from bioenergetics to the metabolic regulation of carcinogenesis, Front Biosci 14 (2009) 4015–4034.
[18] S. Rodriguez-Enriquez, J.C. Gallardo-Perez, A. Aviles-Salas, A. Marin-Hernandez, L. Carreno-Fuentes, V. Maldonado-Lagunas, R. Moreno-Sanchez, Energy metabolism transition in multi-cellular human tumor spheroids, J Cell Physiol 216 (2008) 189–197.
[19] J.M. Cuezva, G. Chen, A.M. Alonso, A. Isidoro, D.E. Misek, S.M. Hanash, D.G. Beer, The bioenergetic signature of lung adenocarcinomas is a molecular marker of cancer diagnosis and prognosis, Carcinogenesis 25 (2004) 1157–1163.
[20] J.M. Cuezva, M. Krajewska, M.L. de Heredia, S. Krajewski, G. Santamaria, H. Kim, J.M. Zapata, H. Marusawa, M. Chamorro, J.C. Reed, The bioenergetic signature of cancer: a marker of tumor progression, Cancer Res 62 (2002) 6674–6681.
[21] R. Rossignol, R. Gilkerson, R. Aggeler, K. Yamagata, S.J. Remington, R.A. Capaldi, Energy substrate modulates mitochondrial structure and oxidative capacity in cancer cells, Cancer Res 64 (2004) 985–993.
[22] K. Smolkova, N. Bellance, F. Scandurra, E. Genot, E. Gnaiger, L. Plecita-Hlavata, P. Jezek, R. Rossignol, Mitochondrial bioenergetic adaptations of breast cancer cells to aglycemia and hypoxia, J Bioenerg Biomembr 42 (2010) 55–67.
[23] L.H. Stockwin, S.X. Yu, S. Borgel, C. Hancock, T.L. Wolfe, L.R. Phillips, M.G. Hollingshead, D.L. Newton, Sodium dichloroacetate selectively targets cells with defects in the mitochondrial ETC, Int J Cancer (2010).
[24] T.J. Schulz, R. Thierbach, A. Voigt, G. Drewes, B. Mietzner, P. Steinberg, A.F. Pfeiffer, M. Ristow, Induction of oxidative metabolism by mitochondrial frataxin inhibits cancer growth: Otto Warburg revisited, J Biol Chem 281 (2006) 977–981.
[25] M. Lagouge, C. Argmann, Z. Gerhart-Hines, H. Meziane, C. Lerin, F. Daussin, N. Messadeq, J. Milne, P. Lambert, P. Elliott, B. Geny, M. Laakso, P. Puigserver, J. Auwerx, Resveratrol improves mitochondrial function and protects against metabolic disease by activating SIRT1 and PGC-1alpha, Cell 127 (2006) 1109–1122.
[26] C. Canto, Z. Gerhart-Hines, J.N. Feige, M. Lagouge, L. Noriega, J.C. Milne, P.J. Elliott, P. Puigserver, J. Auwerx, AMPK regulates energy expenditure by modulating NAD + metabolism and SIRT1 activity, Nature 458 (2009) 1056–1060.
[27] W.W. Winder, B.F. Holmes, D.S. Rubink, E.B. Jensen, M. Chen, J.O. Holloszy, Activation of AMP-activated protein kinase increases mitochondrial enzymes in skeletal muscle, J Appl Physiol 88 (2000) 2219–2226.
[28] L. Yu, S.J. Yang, AMP-activated protein kinase mediates activity-dependent regulation of peroxisome proliferator-activated receptor gamma coactivator-1alpha and nuclear respiratory factor 1 expression in rat visual cortical neurons, Neuroscience 169 (2010) 23–38.
[29] G.K. McConell, G.P. Ng, M. Phillips, Z. Ruan, S.L. Macaulay, G.D. Wadley, Central role of nitric oxide synthase in AICAR and caffeine-induced mitochondrial biogenesis in L6 myocytes, J Appl Physiol 108 (2010) 589–595.
[30] K.S. Persons, V.J. Eddy, S. Chadid, R. Deoliveira, A.K. Saha, R. Ray, Anti-growth effect of 1, 25-dihydroxyvitamin D3-3-bromoacetate alone or in combination with 5-amino-imidazole-4-carboxamide-1-beta-4-ribofuranoside in pancreatic cancer cells, Anticancer Res 30 (2010) 1875–1880.
[31] J. Woodard, L.C. Platanias, AMP-activated kinase (AMPK)-generated signals in malignant melanoma cell growth and survival, Biochem Biophys Res Commun 398 (2010) 135–139.
[32] S.Y. Yu, D.W. Chan, V.W. Liu, H.Y. Ngan, Inhibition of cervical cancer cell growth through activation of upstream kinases of AMP-activated protein kinase, Tumour Biol 30 (2009) 80–85.
[33] T.J. Guan, F.J. Qin, J.H. Du, L. Geng, Y.Y. Zhang, M. Li, AICAR inhibits proliferation and induced S-phase arrest, and promotes apoptosis in CaSki cells, Acta Pharmacol Sin 28 (2007) 1984–1990.
[34] J.H. Jung, J.O. Lee, J.H. Kim, S.K. Lee, G.Y. You, S.H. Park, J.M. Park, E.K. Kim, P.G. Suh, J.K. An, H.S. Kim, Quercetin suppresses HeLa cell viability via AMPK-induced HSP70 and EGFR down-regulation, J Cell Physiol 223 (2010) 408–414.
[35] C. Garcia-Garcia, C. Fumarola, N. Navaratnam, D. Carling, A. Lopez-Rivas, AMPK-independent down-regulation of cFLIP and sensitization to TRAIL-induced apoptosis by AMPK activators, Biochem Pharmacol 79 (2010) 853–863.
[36] R. Rattan, S. Giri, A.K. Singh, I. Singh, 5-Aminoimidazole-4-carboxamide-1-beta-D-ribofuranoside inhibits cancer cell proliferation in vitro and *in vivo* via AMP-activated protein kinase, J Biol Chem 280 (2005) 39582–39593.
[37] T.K. Sengupta, G.M. Leclerc, T.T. Hsieh-Kinser, G.J. Leclerc, I. Singh, J.C. Barredo, Cytotoxic effect of 5-aminoimidazole-4-carboxamide-1-beta-4-ribofuranoside (AICAR) on childhood acute lymphoblastic leukemia (ALL) cells: implication for targeted therapy, Mol Cancer 6 (2007) 46.
[38] D. Guo, I.E. Hildebrandt, R.M. Prins, H. Soto, M.M. Mazzotta, J. Dang, J. Czernin, J.Y. Shyy, A.D. Watson, M. Phelps, C.G. Radu, T.F. Cloughesy, P.S. Mischel, The AMPK agonist AICAR inhibits the growth of EGFRvIII-expressing glioblastomas by inhibiting lipogenesis, Proc Natl Acad Sci USA 106 (2009) 12932–12937.
[39] J. Zhou, W. Huang, R. Tao, S. Ibaragi, F. Lan, Y. Ido, X. Wu, Y.O. Alekseyev, M.E. Lenburg, G.F. Hu, Z. Luo, Inactivation of AMPK alters gene expression and promotes growth of prostate cancer cells, Oncogene 28 (2009) 1993–2002.
[40] X. Xiang, A.K. Saha, R. Wen, N.B. Ruderman, Z. Luo, AMP-activated protein kinase activators can inhibit the growth of prostate cancer cells by multiple mechanisms, Biochem Biophys Res Commun 321 (2004) 161–167.
[41] P. Mukherjee, T.J. Mulrooney, J. Marsh, D. Blair, T.C. Chiles, T.N. Seyfried, Differential effects of energy stress on AMPK phosphorylation and apoptosis in experimental brain tumor and normal brain, Mol Cancer 7 (2008) 37.
[42] P. Baumann, S. Mandl-Weber, B. Emmerich, C. Straka, R. Schmidmaier, Activation of adenosine monophosphate activated protein kinase inhibits growth of multiple myeloma cells, Exp Cell Res 313 (2007) 3592–3603.
[43] R.Y. Su, Y. Chao, T.Y. Chen, D.Y. Huang, W.W. Lin, 5-Aminoimidazole-4-carboxamide riboside sensitizes TRAIL- and TNF{alpha}-induced cytotoxicity in colon cancer cells through AMP-activated protein kinase signaling, Mol Cancer Ther 6 (2007) 1562–1571.
[44] Y.M. Kim, J.T. Hwang, D.W. Kwak, Y.K. Lee, O.J. Park, Involvement of AMPK signaling cascade in capsaicin-induced apoptosis of HT-29 colon cancer cells, Ann NY Acad Sci 1095 (2007) 496–503.
[45] M. Saitoh, K. Nagai, K. Nakagawa, T. Yamamura, S. Yamamoto, T. Nishizaki, Adenosine induces apoptosis in the human gastric cancer cells via an intrinsic pathway relevant to activation of AMP-activated protein kinase, Biochem Pharmacol 67 (2004) 2005–2011.
[46] K. Sai, D. Yang, H. Yamamoto, H. Fujikawa, S. Yamamoto, T. Nagata, M. Saito, T. Yamamura, T. Nishizaki, A(1) adenosine receptor signal and AMPK involving caspase-9/-3 activation are responsible for adenosine-induced RCR-1 astrocytoma cell death, Neurotoxicology 27 (2006) 458–467.
[47] J.V. Swinnen, A. Beckers, K. Brusselmans, S. Organe, J. Segers, L. Timmermans, F. Vanderhoydonc, L. Deboel, R. Derua, E. Waelkens, E. De Schrijver, T. Van de Sande, A. Noel, F. Foufelle, G. Verhoeven, Mimicry of a cellular low energy status blocks tumor cell anabolism and suppresses the malignant phenotype, Cancer Res 65 (2005) 2441–2448.
[48] C. Rocher, J.W. Taanman, D. Pierron, B. Faustin, G. Benard, R. Rossignol, M. Malgat, L. Pedespan, T. Letellier, Influence of mitochondrial DNA level on cellular energy

metabolism: implications for mitochondrial diseases, J Bioenerg Biomembr 40 (2008) 59–67.
[49] E. Borenfreund, J.A. Puerner, Toxicity determined in vitro by morphological alterations and neutral red absorption, Toxicol Lett 24 (1985) 119–124.
[50] K. Nouette-Gaulain, N. Bellance, B. Prevost, E. Passerieux, C. Pertuiset, O. Galbes, K. Smolkova, F. Masson, S. Miraux, J.P. Delage, T. Letellier, R. Rossignol, X. Capdevila, F. Sztark, Erythropoietin protects against local anesthetic myotoxicity during continuous regional analgesia, Anesthesiology 110 (2009) 648–659.
[51] G. Benard, N. Bellance, D. James, P. Parrone, H. Fernandez, T. Letellier, R. Rossignol, Mitochondrial bioenergetics and structural network organization, J Cell Sci 120 (2007) 838–848.
[52] R.J. Youle, M. Karbowski, Mitochondrial fission in apoptosis, Nat Rev Mol Cell Biol 6 (2005) 657–663.
[53] W.J. Ryves, A.J. Harwood, The interaction of glycogen synthase kinase-3 (GSK-3) with the cell cycle, Prog Cell Cycle Res 5 (2003) 489–495.
[54] M. Monk, C. Holding, Human embryonic genes re-expressed in cancer cells, Oncogene 20 (2001) 8085–8091.
[55] D. Kukidome, T. Nishikawa, K. Sonoda, K. Imoto, K. Fujisawa, M. Yano, H. Motoshima, T. Taguchi, T. Matsumura, E. Araki, Activation of AMP-activated protein kinase reduces hyperglycemia-induced mitochondrial reactive oxygen species production and promotes mitochondrial biogenesis in human umbilical vein endothelial cells, Diabetes 55 (2006) 120–127.
[56] R.L. Elstrom, D.E. Bauer, M. Buzzai, R. Karnauskas, M.H. Harris, D.R. Plas, H. Zhuang, R.M. Cinalli, A. Alavi, C.M. Rudin, C.B. Thompson, Akt stimulates aerobic glycolysis in cancer cells, Cancer Res 64 (2004) 3892–3899.
[57] R. Dixon, J. Gourzis, D. McDermott, J. Fujitaki, P. Dewland, H. Gruber, AICA-riboside: safety, tolerance, and pharmacokinetics of a novel adenosine-regulating agent, J Clin Pharmacol 31 (1991) 342–347.
[58] S. Wei, S.K. Kulp, C.S. Chen, Energy restriction as an antitumor target of thiazolidinediones, J Biol Chem 285 (2010) 9780–9791.